# Unified Chassis Control for the Improvement of Agility, Maneuverability, and Lateral Stability

Wanki Cho, Jaewoong Choi, Chongkap Kim, Seibum Choi, and Kyongsu Yi

***Abstract*—This paper describes a unified chassis control (UCC) strategy for improving agility, maneuverability, and vehicle lateral stability by the integration of active front steering (AFS) and electronic stability control (ESC). The proposed UCC system consists of a supervisor, a control algorithm, and a coordinator. The supervisor determines the target yaw rate and velocity based on control modes that consist of no-control, agility-control, maneuverability-control, and lateral-stability-control modes. These control modes can be determined using indices that are dimensionless numbers to monitor a current driving situation. To achieve the target yaw rate and velocity, the control algorithm determines the desired yaw moment and longitudinal force, respectively. The desired yaw moment and longitudinal force can be generated by the coordination of the AFS and ESC systems. To consider a performance limit of the ESC system and tires, the coordination is designed using the Karush–Kuhn–Tucker (KKT) condition in an optimal manner. Closed-loop simulations with a driver–vehicle–controller system were conducted to investigate the performance of the proposed control strategy using the CarSim vehicle dynamics software and the UCC controller, which was coded using MATLAB/Simulink. Based on our simulation results, we show that the proposed UCC control algorithm improves vehicle motion with respect to agility, maneuverability, and lateral stability, compared with conventional ESC.**

***Index Terms*—Active front steering (AFS), agility, electronic stability control (ESC), lateral stability, maneuverability, unified chassis control (UCC).**

## NOMENCLATURE

| | |
|---|---|
| $a_x$ | Vehicle longitudinal acceleration. |
| $a_y$ | Vehicle lateral acceleration. |
| $l_f$ | Distance from the center of gravity (CG) to front axle = 1.07 m. |
| $l_r$ | Distance from the CG to rear axle = 1.78 m. |
| $m$ | Total mass of the vehicle = 2450 kg. |
| $t_f$ | Tread (track width) = 1.62 m. |
| $C_{f,A}$ | Front tire cornering stiffness for agility. |
| $C_{f,M}$ | Front tire cornering stiffness for maneuverability = 7.2699e + 004 N/rad. |
| $C_r$ | Rear tire cornering stiffness = 5.8868e + 004 N/rad. |
| $F_x$ | Desired longitudinal force. |
| $F_{x,FL}$ | Longitudinal tire force of the front-left wheel. |
| $F^*_{x,FL}$ | Longitudinal tire force of the front-left wheel by the ESC. |
| $F_{x,FR}$ | Longitudinal tire force of the front-right wheel. |
| $F^*_{x,FR}$ | Longitudinal tire force of the front-right wheel by the ESC. |
| $F_{x,RL}$ | Longitudinal tire force of the rear-left wheel. |
| $F^*_{x,RL}$ | Longitudinal tire force of the rear-left wheel by the ESC. |
| $F_{x,RR}$ | Longitudinal tire force of the rear-right wheel. |
| $F^*_{x,RR}$ | Longitudinal tire force of the rear-right wheel by the ESC. |
| $F_{y,FL}$ | Lateral tire force of the front-left wheel. |
| $F^*_{y,FL}$ | Lateral tire force of the front-left wheel by the AFS. |
| $F_{y,FR}$ | Lateral tire force of the front-right wheel. |
| $F^*_{y,FR}$ | Lateral tire force of the front-right wheel by the AFS. |
| $F_{y,RL}$ | Lateral tire force of the rear-left wheel. |
| $F_{y,RR}$ | Lateral tire force of the rear-right wheel. |
| $F_{z,FL}$ | Vertical force of the front-left wheel. |
| $F_{z,FR}$ | Vertical force of the front-right wheel. |
| $F_{z,RL}$ | Vertical force of the rear-left wheel. |
| $I_z$ | Moment of inertia about yaw axis (o) = 4331.6 kg m2. |
| $M_Z$ | Desired yaw moment. |
| $V_x$ | Vehicle longitudinal velocity, positive forward. |
| $V_y$ | Vehicle lateral velocity, positive toward left. |
| $\alpha_f$ | Slip angle of the front tire. |
| $\alpha_r$ | Slip angle of the rear tire. |
| $\beta$ | Vehicle sideslip angle. |
| $\delta_f$ | Tire steer angle. |
| $\gamma$ | Yaw rate. |
| $\gamma_{des}$ | Target yaw rate. |
| $\gamma_{des,A/M}$ | Target yaw rate for agility and maneuverability. |
| $\gamma_{des,L}$ | Target yaw rate for lateral stability. |
| $\mu$ | Tire–road friction coefficient. |

Manuscript received March 16, 2011; revised July 21, 2011 and October 24, 2011; accepted December 27, 2011. Date of publication January 9, 2012; date of current version March 21, 2012. This work was supported in part by the Hyundai Motor Company through the BK21 Program, the Institute of Advanced Machinery and Design, Seoul National University, the Korean Government under the Ministry of Education, Science and Technology through the Korea Research Foundation Grant under Contract KRF-2009-200-D00003, and the National Research Foundation of Korea, funded by the Korean Government, under Grant 2010-0001958. The review of this paper was coordinated by Prof. L. Guvenc.

W. Cho, J. Choi, and K. Yi are with the School of Mechanical and Aerospace Engineering, Seoul National University, Seoul 151-742, Korea (e-mail: nawanki0@ snu.ac.kr; loar00@snu.ac.kr; kyi@snu.ac.kr).

C. Kim is with the Intelligent Vehicle Safety System Development Team, Hyundai Motor Company, Seoul 137-938, Korea (e-mail: ckkim@ hyundai.com).

S. Choi is with the Department of Mechanical Engineering, Korea Advanced Institute of Science and Technology, Daejeon 305-701, Korea (e-mail: sbchoi@kaist.ac.kr).

Color versions of one or more of the figures in this paper are available online at http://ieeexplore.ieee.org.

Digital Object Identifier 10.1109/TVT.2012.2183152

## I. Introduction

To IMPROVE the handling performance and active safety of vehicles, numerous active control systems for vehicle lateral dynamics have been developed and commercialized over the last two decades. Electronic stability control (ESC) is the most popular system, and it is well recognized that ESC can significantly improve vehicle lateral stability for a wide range of critical driving situations. Recent studies have shown that the integration of individual modular chassis control systems such as ESC, active front steering (AFS), four-wheel drive (4WD), continuous damping control (CDC), and active roll control (ARC) is the most efficient way of enhancing vehicle dynamics characteristics such as agility, maneuverability, and additional stability improvement. Recently, the integration of individual modular chassis control systems to increase handling performance and vehicle stability has been investigated by several researchers. The coordination of steering and individual wheel braking actuation to achieve better vehicle yaw stability has been reported [1]. Intelligent vehicle motion control that interfaces a theoretical controller with existing braking and steering chassis subsystems has been proposed [2]. The linear quadratic (LQ) control theory has been applied to the design of the integrated direct yaw moment (DYM) and AFS [3]. This control system was designed using a model-matching control technique that makes the performance of the actual vehicle model follow an ideal vehicle model. An integrated chassis control system that consists of an ESC integrated differential braking function and a CDC suspension function for the worst case was introduced in [4]. Fuzzy logic and the LQ control theory have been applied to the design of combined direct yaw moment control (DYC) and an active steering system [5]. The yaw stability enhancement of vehicles through combined differential braking and active rear steering (ARS) system has been investigated [6]. An integrated vehicle chassis control algorithm based on the basis of tire force correlativity has been designed by the coordination of active suspension and four-wheel steering (4WS) to improve vehicle ride and handling [7]. A coordinated vehicle dynamics control approach with individual wheel torque and steering actuation was investigated in [8]. In this approach, a weighted pseudo inverse-based control allocation method is employed for a computationally efficient distribution of the control of slip ratio and the slip angle of each wheel. To reduce the negative effects of dynamics coupling among vehicle subsystems and improve the handling performance of a vehicle under severe driving conditions, a vehicle chassis integration approach based on a main- and servo-loop structure has been proposed [9]. To optimize tire usage to achieve a target vehicle response, an optimum longitudinal and lateral tire force distribution through four-wheel independent steering, driving, and braking has been proposed [10]. To maximize the stability limit and vehicle responsiveness, a vehicle dynamics integrated control algorithm using an online nonlinear optimization method has been proposed for four-wheel-distributed steering and four-wheel-distributed traction/braking systems [11]. The functional integration of vehicle dynamics control systems applied to active suspension and slip control is investigated in [12].

The integration of individual modular chassis control systems can provide additional benefits for vehicle dynamics such as agility, maneuverability, and vehicle lateral stability compared to a conventional ESC system. This paper presents a unified chassis control (UCC) strategy for improving agility, maneuverability, and lateral stability. For the more dynamic motion than the standard motion, which is determined by the tire characteristic, the agility function is added in the UCC system. Agility is defined as the neutral steer, which is an ideal state of balance. Because excessive body sideslip of a vehicle makes the yaw motion insensitive to a driver's steering input and causes deterioration in lateral stability, lateral stability function for body sideslip is also added. Lateral stability is defined in this paper as the body sideslip angle over a reasonably small range. To satisfy these functions, target vehicle motions such as yaw rate and velocity are determined based on the indices for monitoring the current driving situation. To track the target motions, the desired yaw moment and longitudinal force are calculated. In the case of conventional ESC, because the desired yaw moment and longitudinal force are generated only by differential braking, if there is no deceleration demand by the driver, the decelerations of the vehicle due to the differential braking for yaw stability control have a negative effect on the conventional ESC. To solve this problem, the coordinator manipulates a brake and steering actuators. Finally, the performance of the proposed control algorithm is verified using closed-loop simulation for several driving situations.

## II. Unified Chassis Control Architecture

Fig. 1 shows the UCC architecture proposed in this paper. As shown in the figure, the architecture consists of the following two parts: 1) an estimator and 2) a UCC controller. For the implementation of the proposed UCC, the longitudinal, lateral, and vertical tire forces and the tire–road friction coefficient are very important. However, these values are very difficult or expensive to directly measure. The tire–road friction coefficient can successfully be estimated in real time using measurements that are available from existing vehicle sensors such as the wheel speed sensor, accelerometers, and engine speed and turbine speed revolutions-per-minute sensor. The longitudinal/lateral/vertical tire force estimation consists of the following five steps, as described in a previous study [13]:

1) vertical tire force estimation;
2) shaft torque estimation;
3) longitudinal tire force estimation based on a simplified wheel dynamics model;
4) lateral tire force estimation based on a planar model;
5) combined tire force estimation.

The UCC controller was designed in the following three stages: 1) a supervisor; 2) a control algorithm; and 3) a coordinator. The supervisor determines target vehicle motions such as the target yaw rate, considering agility for neutral steer; maneuverability; vehicle lateral stability; and the target velocity for the foot pedal position determined by a driver's intention. In addition, to determine optimal target vehicle motions, indices for the correct judgment of the current driving situation

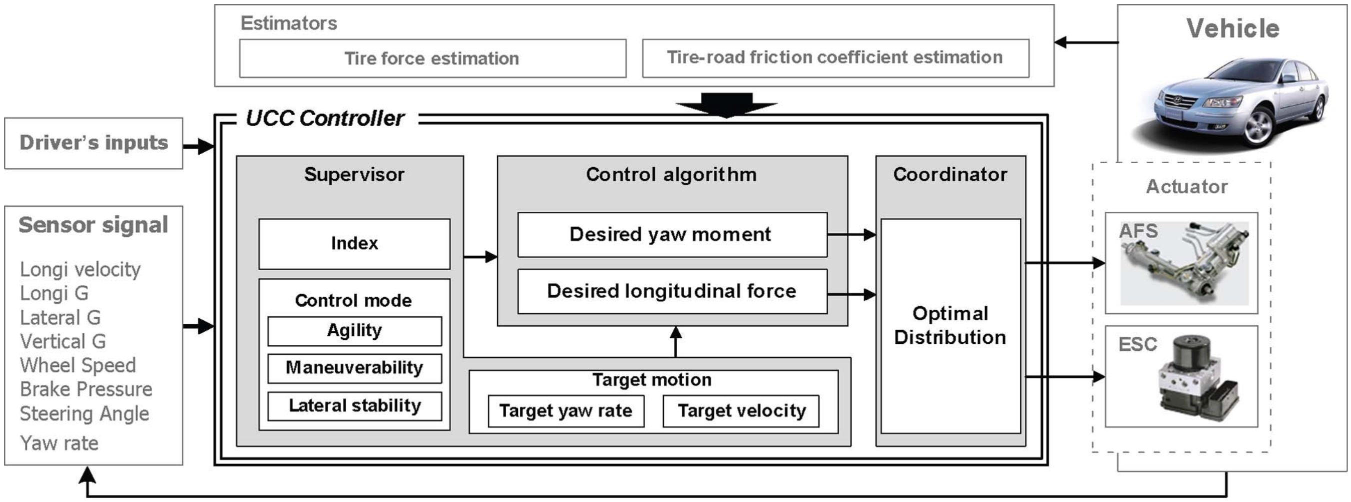


Fig. 1. UCC architecture.

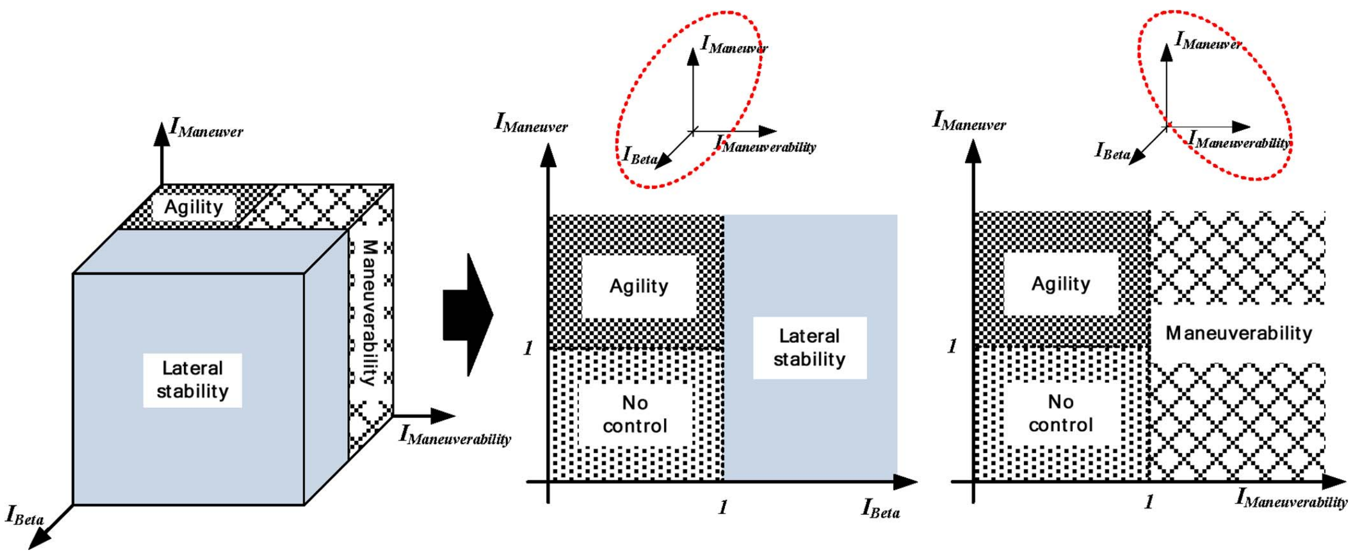


Fig. 2. UCC strategy.

are calculated. Based on this information, yaw moment control based on a 2-D bicycle model was used for agility, maneuverability, and lateral stability. To consider tire cornering stiffness uncertainties, this control method was designed using the sliding-mode control method. Longitudinal force control to track the target velocity was also designed using the sliding-mode control method. Based on the desired longitudinal force and yaw moment, the coordinator optimally distributes actuator inputs based on the current status of the vehicle. The optimal distribution law, considering the performance limit of the ESC system and the tire, is designed.

## III. Supervisor

From the viewpoint of vehicle dynamics, the yaw rate and sideslip angle are closely related to vehicle agility, maneuverability, and lateral stability. The supervisor determines target motions, such as the target yaw rate for the improvement of the agility, maneuverability, and lateral stability, and the target velocity to reflect the driver's intention. To improve the agility, maneuverability, and lateral stability of the vehicle, four control modes (no control, agility control, maneuverability control, and lateral-stability control) can be determined by the indices that are dimensionless numbers for monitoring a current driving situation. To determine the control mode, the following three indices are proposed in this paper: 1) a maneuver index $I_{Maneuver}$; 2) a maneuverability index $I_{Maneuverability}$; and 3) a beta index $I_{Beta}$. The $I_{Maneuver}$, $I_{Maneuverability}$ and $I_{Beta}$ indices are dimensionless numbers for illustrating the current driving situation. If they exceed the unit, they indicate a driver's cornering intention, vehicle unstable motion by the agility control, and a danger of a large vehicle sideslip angle, respectively. Because $I_{Beta}$ was developed in previous research [15], $I_{Maneuver}$ and $I_{Maneuverability}$ will be described in this paper. According to the determined control modes based on the indices, the supervisor calculates the target yaw rate for agility, maneuverability, and lateral stability and the target velocity to reflect the driver's intention.

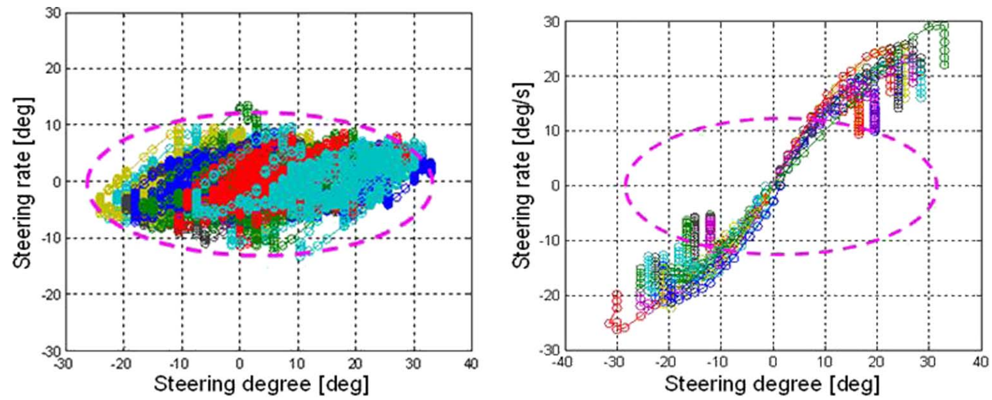


Fig. 3. Steering angle and the steering rate plane in various driving situations. (a) Lane-keeping situations. (b) Lane-change situations.

### A. Control Mode Based on Indices

Fig. 2 shows the control-mode-switching strategy. The indices are used for switching between control modes. For example, $I_{Maneuver}$ is used for switching between the no- and agility-control modes, and $I_{Maneuverability}$ is used between the agility- and maneuverability-control modes. As shown in the figure, each control mode is activated on the order of priority to lateral stability, maneuverability, and agility.

$I_{Beta}$ is a dimensionless number that can indicate the danger of a large vehicle sideslip angle and can be calculated using the phased plane for $\beta - \dot{\beta}$ as follows [15]:

$$I_{Beta} = |a\beta + b\dot{\beta}| \tag{1}$$

where $a$ and $b$ are tuning parameters that can be determined under several driving conditions.

In general, a driver operates the steering wheel angle to maintain the vehicle's position, even in a straight lane. In this driving situation, because a driver does not have a cornering intention, an agility control can lead to a negative effect for the driver. Thus, $I_{Maneuver}$ for deciding the driver's cornering intention is developed in this paper. $I_{Maneuver}$ is used to determine the threshold between the no- and the agility-control modes. $I_{Maneuver}$ can be determined using experimental data [16]. Fig. 3 shows the experimental data used to determine $I_{Maneuver}$. Fig. 3(a) and (b) shows the steering angle and the steering angle rate planes for lane keeping and lane change in a straight lane, respectively. During lane keeping, i.e., the driver does not have a cornering intention, the regions of the steering angle and the steering angle rate are within the threshold value (indicated in the figure as a magenta dashed line). On the contrary, in a lane change, i.e., the driver has a cornering intention, the regions exceed the threshold value.

Therefore, $I_{Maneuver}$ can be determined by experimental results. Fig. 4 shows the strategy for the determination of $I_{Maneuver}$. The experimental data for lane keeping are used to develop $I_{Maneuver}$. If the absolute values of the steering angle and steering angle rate are within the yellow region, $I_{Maneuver}$ is calculated below the unit, because the driver does not have a cornering intention. On the contrary, exceeding the yellow region, $I_{Maneuver}$ should exceed the unit.

Therefore, $I_{Maneuver}$ can be calculated as follows:

$$\mathrm{I_{maneuve}} = \frac{\mathrm{L2}}{\mathrm{L1}} = \frac{c|\dot{\delta}_f| + d|\delta_f|}{c^2}. \tag{2}$$

$I_{Maneuverability}$ is the threshold value used to determine the control mode between agility control and maneuverability control. In the agility-control mode, for the more dynamical motion of the vehicle, the target yaw rate for neutral steer is determined. Neutral steer is a cornering condition in which the front and rear slip angles are roughly the same. The neutral steer motion results in more oversteer than the standard target motion, which is determined by tire characteristics. Thus, in the case of agility control, because the target yaw rate for agility more quickly exceeds the limit of the yaw rate than for maneuverability, the control mode should be changed from agility to maneuverability before the target yaw rate for agility exceeds the limit of the yaw rate. Therefore, $I_{Maneuverability}$ is determined using the target yaw rate for agility and the yaw rate threshold value, which is the limit of the yaw rate calculated by the tire–road friction coefficient and velocity [19]. Fig. 5 shows the yaw rate threshold value for the velocity. As shown in this figure, if the target yaw rate for agility exceeds the limit of the yaw rate, maneuverability control will be activated. Therefore, $I_{Maneuverability}$ can be determined by dividing the target yaw rate for agility by the yaw rate threshold. In addition, to avoid a discrete change of two target yaw rates for the agility and maneuverability modes, a switching region for $I_{Maneuverability}$ was used. The blue dotted line in Fig. 5 is the switching start point and is set to be a half value of the yaw rate threshold.

Based on Fig. 5, $I_{Maneuverability}$ is calculated as follows:

$$\mathrm{I_{maneuverability}} = \frac{\gamma_{des,A}}{\gamma_{threshold}} \tag{3}$$

where $\gamma_{des,A}$ and $\gamma_{threshold}$ are the target yaw rate for the improvement of agility and the yaw rate threshold, respectively.

### B. Target Vehicle Motion

Suitable target vehicle motions such as yaw rate and velocity are determined based on the developed indices. For the improvement of agility, maneuverability, and lateral stability, considering a driver's intention for deceleration/acceleration,

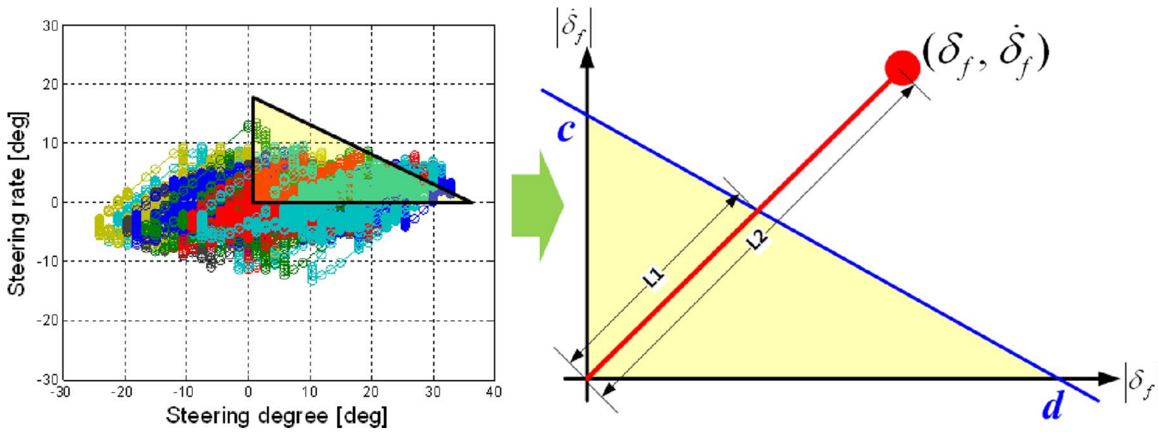


Fig. 4. Strategy for the determination of $I_{Maneuver}$.

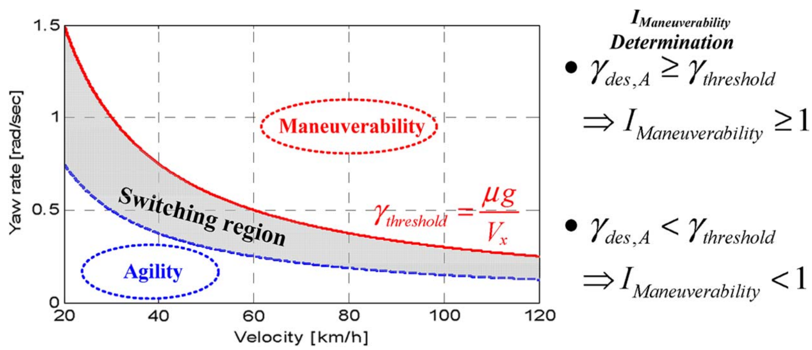


Fig. 5. Yaw rate threshold value for the velocity.

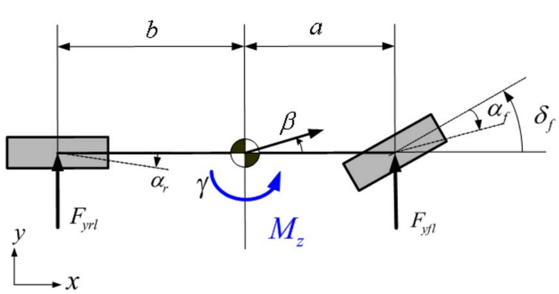


Fig. 6. Two-dimensional bicycle model, including the DYM.

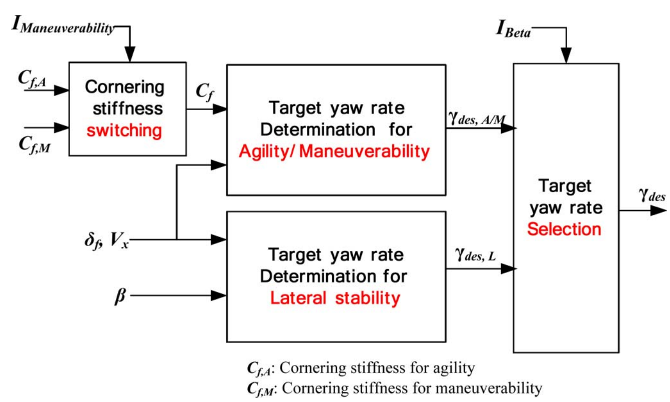


Fig. 7. Determination scheme of the target yaw rate for agility, maneuverability, and lateral stability.

we propose an approach for yaw rate and velocity control. In the yaw rate control, the target yaw rate was determined using a 2-D bicycle model. Velocity control determines the target velocity based on the driver's foot pedal position. Fig. 6 shows a 2-D bicycle model, including a DYM. This model can represent the vehicle dynamics in the region of linear tire characteristics and has been validated in many publications in the literature [3].

The corresponding dynamic equations are

$$\begin{bmatrix} \dot{\beta} \\ \dot{\gamma} \end{bmatrix} = \begin{bmatrix} \frac{-2(C_f + C_r)}{mV_x} & \frac{2(-l_f C_f + l_r C_r)}{mV_x^2} - 1 \\ \frac{2(-l_f C_f + l_r C_r)}{I_z} & \frac{-2(l_f^2 C_f + l_r^2 C_r)}{I_z V_x} \end{bmatrix} \begin{bmatrix} \beta \\ \gamma \end{bmatrix} + \begin{bmatrix} \frac{2C_f}{mv_x} \\ \frac{2l_f C_f}{I_z} \end{bmatrix} \delta_f + \begin{bmatrix} 0 \\ \frac{1}{I_z} \end{bmatrix} M_z \tag{4}$$

$$a_y = V_x(\dot{\beta} + \gamma). \tag{5}$$

Fig. 7 shows the proposed target yaw rate determination scheme for agility, maneuverability, and lateral stability. The target yaw rates for agility and maneuverability are determined by the steady-state value for the yaw rate dynamics of the bicycle model. To separate the target yaw rates for agility and maneuverability, two types of the front tire's cornering stiffness are used. The switching time between agility and maneuverability is determined by $I_{Maneuverability}$. The target yaw rate for lateral stability is calculated from the beta dynamics of the bicycle model. Based on the two determined target yaw rates, the final target yaw rate is determined by $I_{Beta}$.

The target yaw rate can be determined by a combination of two different target yaw rates as follows:

$$\gamma_{des} = \sigma\gamma_{des,A/M} + (1-\sigma)\gamma_{des,L}, \quad \text{where} \quad 0 \le \sigma \le 1 \tag{6}$$

where $\gamma_{des,A/M}$ and $\gamma_{des,L}$ are the target yaw rates for agility/maneuverability and lateral stability, respectively, and $\sigma$ is a weighting factor determined by $I_{Beta}$. When $I_{Beta}$ is smaller than the specified threshold value, $\sigma$ is set to 1 to improve vehicle agility or maneuverability. When $I_{Beta}$ is larger than the specified threshold value, $\sigma$ is set to 0 to improve vehicle lateral stability. To avoid a discrete change between two target yaw rates in the threshold region of $I_{Beta}$, weighting factors that consist of a linear function about $I_{Beta}$ were determined.

The target yaw rate for agility and maneuverability can be determined using the steady-state value of the yaw rate dynamics from the bicycle model. To determine two target yaw rates for agility and maneuverability, two different cornering stiffness values of the front tire were used. For agility control, the cornering stiffness of the front tire $C_f$ for neutral steer is used. Neutral steer means that the front and rear tires have the same tire slip angle, i.e.,

$$\alpha_f = \alpha_r. \tag{7}$$

The tire slip angles can be represented as the relationship between the lateral force and the cornering stiffness, and the lateral force can be calculated using the lateral and yaw acceleration [15]. Therefore, the tire slip angles can be determined as follows:

$$\alpha_f = \frac{F_{yf}}{C_{f,A}} = \frac{l_r m a_y + I_z\dot{\gamma}}{(l_r+l_f)C_{f,A}}, \quad \alpha_r = \frac{F_{yr}}{C_r} = \frac{l_f m a_y - I_z\dot{\gamma}}{(l_r+l_f)C_r}. \tag{8}$$

For the steady-state case, the yaw acceleration $(\dot{\gamma})$ described in (8) is set to zero. Substituting (8) into (7), the resulting equation is expressed as follows:

$$\frac{l_r m a_y}{(l_r+l_f)C_{f,A}} = \frac{l_f m a_y}{(l_r+l_f)C_r}. \tag{9}$$

Based on (9), the cornering stiffness of the front tire for neutral steer can be expressed as follows:

$$C_{f,A} = \frac{l_r}{l_f}C_r. \tag{10}$$

In the case of maneuverability control, the cornering stiffness $(C_{f,M})$ of the front tire, which is tuned by the tire characteristic of the vehicle, was used in (6). Based on $I_{Maneuverability}$, two different tire cornering stiffness were combined into a single cornering stiffness as follows:

$$C_f = \rho C_{f,A} + (1-\rho)C_{f,M}. \tag{11}$$

The weighting factor $\rho$ used in (11) can be determined using $I_{Maneuverability}$, as shown in Fig. 8.

Based on the calculated cornering stiffness and (4), the target yaw rate for agility and maneuverability based on the driver's steering input is theoretically determined in light of the 2-D bicycle model with a linear tire force. The steady-state yaw rate of the bicycle model is introduced, and the maneuver of the vehicle is considered to reflect the driver's intentions, which is expressed as a function of the vehicle's longitudinal velocity and the driver's steering input as follows [18]:

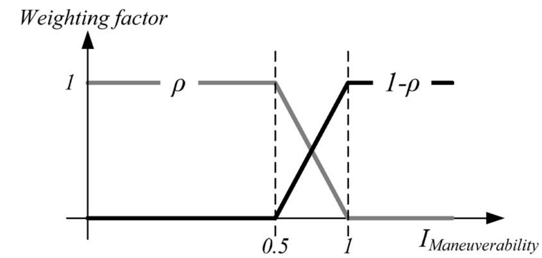


Fig. 8. Control-mode-switching strategy between agility and maneuverability.

$$\gamma_{des,A/M} = \frac{1}{1 - \frac{m(l_f C_f - l_r C_r)V_x^2}{2C_f C_r (l_f+l_r)^2}} \frac{V_x}{l_f + l_r}\delta_f. \tag{12}$$

The target yaw rate for lateral stability, which is required to maintain the sideslip angle in a reasonably small range, is calculated using the beta dynamics of the bicycle model as follows [15]:

$$\gamma_{des,L} = K_1\beta + \frac{(F_{y,FL}+F_{y,FR})\cos\delta_f + (F_{y,RL}+F_{y,RR})}{mV_x}. \tag{13}$$

Then, the sideslip angle changes to a stable dynamics condition, as shown in (13). This case implies that the body sideslip angle asymptotically converges to zero. Thus, we have

$$\dot{\beta} = -K_1\beta \tag{14}$$

where $K_1$ is a design parameter that is strictly positive.

In the case of the target velocity, for an acceleration or deceleration maneuver, the target longitudinal acceleration can be detected from the foot pedal position. Therefore, neglecting the delay effort of the driver's response, the target velocity can be written as follows [9]:

$$V_{x,des} = V_x + \int_0^t a_{x,des}(\tau)\, d(\tau). \tag{15}$$

## IV. Control Algorithm

The control algorithm determines the desired yaw moment for the yaw rate control and the desired longitudinal force for the velocity control. The purpose of the desired yaw moment is to reduce the yaw rate error between the actual and the target yaw rate determined in Section III-B. To calculate the desired yaw moment, using (4) and (5), the bicycle model can be rewritten by eliminating the body sideslip angle as follows [17]:

$$\dot{\gamma} = -\frac{2C_f C_r}{C_f + C_r}\frac{(l_f+l_r)^2}{I_Z V_x}\gamma + \frac{m(l_f C_f - l_r C_r)}{(C_f+C_r)I_Z}a_y + \frac{2C_f C_r}{C_f+C_r}\frac{(l_f+l_r)}{I_Z}\delta_f + \frac{1}{I_Z}M_Z. \tag{16}$$

The sliding-mode control method is used to determine the desired yaw moment, considering uncertainties of the cornering stiffness. The sliding surface and the sliding condition are defined as follows:

$$S_1 = \gamma_x - \gamma_{x,des}, \qquad \dot{S}_1 S_1 \le -\eta_1 |S_1|. \tag{17}$$

The equivalent control input that would achieve $\dot{S}_1 = 0$ is calculated as follows:

$$M_{Z,eq} = I_Z \left( \frac{2\hat{C}_f \hat{C}_r}{\hat{C}_f + \hat{C}_r} \frac{(l_f + l_r)^2}{I_Z V_x} \gamma - \frac{m(l_f \hat{C}_f - l_r \hat{C}_r)}{(\hat{C}_f + \hat{C}_r) I_Z} a_y \right.$$
$$\left. - \frac{2\hat{C}_f \hat{C}_r}{\hat{C}_f + \hat{C}_r} \frac{(l_f + l_r)}{I_Z} \delta_f + \dot{\gamma}_{des} \right). \tag{18}$$

Finally, the desired yaw moment for satisfying the sliding condition, regardless of the model uncertainty, is determined as follows:

$$M_Z = M_{Z,eq} - k_1 sat \left( \frac{\gamma - \gamma_{des}}{\Phi_1} \right). \tag{19}$$

The gain $k_1$, which satisfies the sliding condition, is calculated as follows:

$$k_1 = \left| \frac{2\hat{C}_f \hat{C}_r}{\hat{C}_f + \hat{C}_r} - \frac{2C_f C_r}{C_f + C_r} \right| \left| \frac{(l_f + l_r)^2}{I_Z V_x} \gamma \right|$$
$$+ \left| \frac{2\hat{C}_f \hat{C}_r}{\hat{C}_f + \hat{C}_r} - \frac{2C_f C_r}{C_f + C_r} \right| \left| \frac{(l_f + l_r)}{I_Z} \delta_f \right|$$
$$+ \left| \frac{l_f C_f - l_r C_r}{C_f + C_r} - \frac{l_f \hat{C}_f - l_r \hat{C}_r}{\hat{C}_f + \hat{C}_r} \right| \left| \frac{m}{I_Z} a_y \right| + \eta_1. \tag{20}$$

A detailed description for the determination of the desired yaw moment is provided in previous research [19].

The desired longitudinal force to yield the target vehicle velocity is calculated using a planar model and a sliding-mode control law [18]. The dynamic equation for the $x$-axis of the planar model is described as follows:

$$\dot{V}_x = \frac{1}{m}(F_{x,FL} + F_{x,FR} + F_{x,RL} + F_{x,RR} - F_{yf}\delta_f)$$
$$+ V_y \gamma - \frac{1}{m} F_x. \tag{21}$$

The sliding-mode control method is also used to determine the desired longitudinal force. The sliding surface and the sliding condition are defined as follows:

$$S_2 = V_x - V_{x,des} \qquad \dot{S}_2 S_2 \le -\eta_2 |S_2| \tag{22}$$

where $\eta_2$ is a positive constant. The equivalent control input that would achieve $\dot{S}_2 = 0$ is calculated as follows:

$$F_{x,eq} = (F_{x,FL} + F_{x,FR} + F_{x,RL} + F_{x,RR} - F_{yf}\delta_f)$$
$$+ m(V_y \gamma - \dot{V}_{x,des}). \tag{23}$$

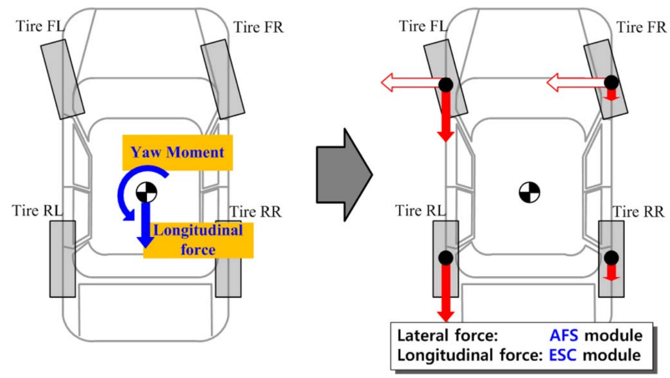


Fig. 9. Coordinate system that corresponds to the resulting force.

Finally, the desired longitudinal force to satisfy the sliding condition is given by

$$F_x = F_{x,eq} - k_2 \cdot sat \left( \frac{V_x - V_{x,des}}{\Phi} \right) \tag{24}$$

where the gain $k_2$, which satisfies the sliding condition, is calculated as follows:

$$k_2 \le -\eta_2 \cdot m. \tag{25}$$

A detailed description of the desired longitudinal force for the target velocity is provided in our previous research [18].

## V. Coordinator

Based on the desired longitudinal force and yaw moment, the coordinator manipulates a brake and the steering actuator. In a conventional ESC, the desired yaw moment and longitudinal force are generated by differential braking. Because differential braking leads to significant longitudinal decelerations and pitching motions of the vehicle body, if the driver does not intend to decelerate, there could be a negative effect on the driver. The desired yaw moment by the AFS could be a solution to this problem. Therefore, an optimized coordination of the AFS and ESC has been proposed in this paper. The optimized coordination determines control inputs that quickly satisfy both the desired yaw moment and longitudinal force. However, if both conditions cannot be satisfied, one of the two conditions should be eliminated. For example, if the deceleration for the remaining yaw moment (which cannot be generated by the AFS due to constraints) is greater than the deceleration specified by the driver's intention, the braking force for the yaw moment control should have control authority. The cost function and the constraints for this condition will be defined in this section.

In the optimization, it was assumed that the maximum values of the lateral tire forces are proportional to the vertical loads of tires and the coefficient of the tire–road friction is sufficiently well estimated. The optimized coordination of the active lateral and longitudinal tire forces $(F_{x,i}, F_{y,i}, i = FL, FR, RL, RR)$ for the desired yaw moment and longitudinal force were determined using the Karush–Kuhn–Tucker (KKT) conditions. Fig. 9 shows the coordinate system that corresponds to the resulting force. The active forces were computed based on the sign of the desired yaw moment.

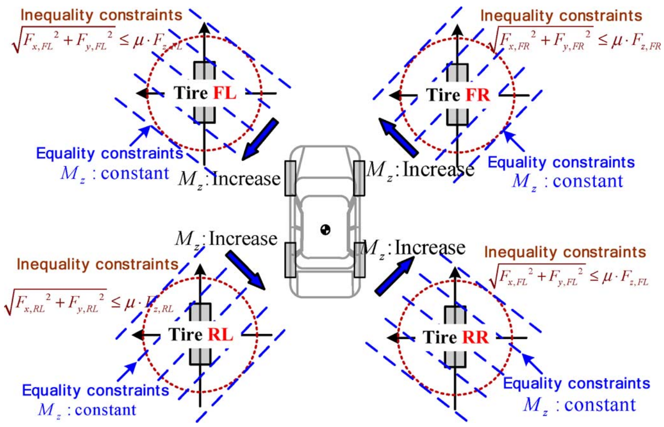


Fig. 10. Constraints of each wheel.

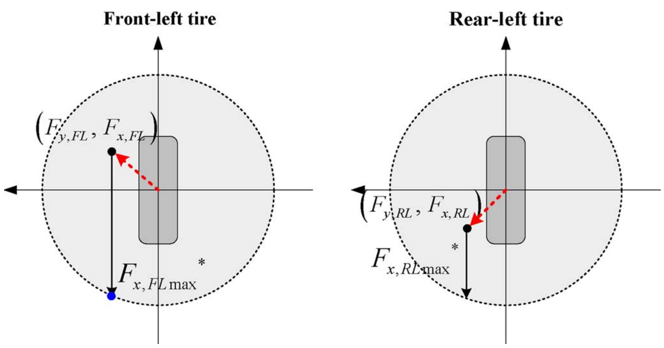


Fig. 11. Friction circles of the front-left and rear-left tires.

When the desired yaw moment is positive, the six active longitudinal and lateral tire forces $(F^*_{x,FL}, F^*_{x,FR}, F^*_{x,RL}, F^*_{x,RR}, F^*_{y,FL}, F^*_{y,FR})$ can be used to generate the desired yaw moment and longitudinal force. To optimize active tire forces, the constraints of each wheel should be determined based on the vertical load, tire–road friction coefficient, desired yaw moment, and desired longitudinal force. Fig. 10 shows the constraints of each wheel for the positive desired yaw moment.

For optimization with the six variables, it is necessary to simplify the optimization because of excessive computational load. This problem can be solved by eliminating variables: three of the six variables can be eliminated based on certain assumptions.

Because the same active steering angle is used for both front tires, the active lateral force for the front-right tire $(F^*_{y,FR})$ can be represented as

$$F^*_{y,FR} = \frac{F_{z,FR}}{F_{z,FL}} F^*_{y,FL}. \tag{26}$$

The active longitudinal force for the rear-left tire $(F^*_{x,RL})$ can be determined using the following braking force distribution strategy for the rear tire. Fig. 11 shows friction circles of the front-left and rear-left tires. Tractive force that is determined by the shaft torque is applied at the front tire, and drag force is applied at the rear tire.

It is assumed that the road friction about the $x$- and $y$-axes can be estimated and the maximum brake forces of the front-left and rear-left tires can be determined as follows:

$$F^*_{x,FL\ \max} = -F_{x,FL} - \sqrt{(\mu F_{z,FL})^2 - (F_{y,FL})^2} \tag{27}$$

$$F^*_{x,RL\ \max} = -F_{x,RL} - \sqrt{(\mu F_{z,RL})^2 - (F_{y,RL})^2}. \tag{28}$$

The braking force distributions of the front-left and rear-left tires are determined using (27) and (28) as follows:

$$F^*_{x,RL} = \frac{|F^*_{x,RL\ \max}|}{|F^*_{x,FL\ \max}|} \cdot F^*_{x,FL}. \tag{29}$$

Using the aforementioned procedures, the braking force distributions on the right side is characterized as follows:

$$F^*_{x,RR} = \frac{|F^*_{x,RR\ \max}|}{|F^*_{x,FR\ \max}|} \cdot F^*_{x,FR}. \tag{30}$$

Three of the six variables $(F^*_{x,RL}, F^*_{x,RR}, F^*_{y,FR})$ can be eliminated from the optimization problem. Therefore, the optimal distribution problem for the active lateral and longitudinal tire forces can be stated as follows:

Cost function

$$L = \left(D_1 F^*_{x,FL} + D_2 F^*_{x,FR} - F_x\right)^2 + \left(D_2 F^*_{x,FR} - \frac{F_x}{2} - \frac{1}{t_f} M_Z\right)^2 \tag{31}$$

subject to

$$\begin{aligned} f_1 &= -\frac{t_f}{2} D_1 F^*_{x,FL} + \frac{t_f}{2} D_2 F_{x,FR*} \\ &\quad + l_f E_1 F_{y,FL*} - M_Z = 0 \\ g_1 &= F^{*2}_{x,FL} + \left(F_{y,FL} + F^*_{y,FL}\right)^2 - \mu^2 \cdot F^2_{z,FL} \le 0 \\ g_3 &= F^*_{x,FR} \le 0 \end{aligned} \tag{32}$$

where $D_1 = 1 + |F^*_{x,RL\ \max}|/|F^*_{x,FL\ \max}|$, $D_2 = 1 + |F^*_{x,RR\ \max}|/|F^*_{x,FR\ \max}|$, and $E_1 = 1 + F_{z,FR}/F_{z,FL}$.

Equation (31) shows a cost function of the optimized coordination. Equation (32) represents an equality constraint for the desired yaw moment and inequality constraints for the performance limits of a tire and the ESC actuator with only differential braking, respectively. In case of zero throttle or acceleration by the driver, because the engine cannot be controlled in this system, the desired longitudinal force for the acceleration was set to zero. Therefore, the cost function means that, if a driver does not have a deceleration intention, the deceleration should be minimized. In this situation, the actuator inputs to minimize the longitudinal tire force are determined by the cost function. This description can be deduced from Fig. 12, which shows a cost value in the yaw moment control case without deceleration control $(M_z > 0, F_x = 0)$. As shown in the figure, considering the inequality constraint for the performance limit of the actuator $(F^*_{x,FR} \le 0)$, the cost value for minimizing the longitudinal tire force will be obtained. In this case, the active steering angle by the AFS is first used to satisfy the desired yaw moment. Then, if the AFS system is insufficient to satisfy the

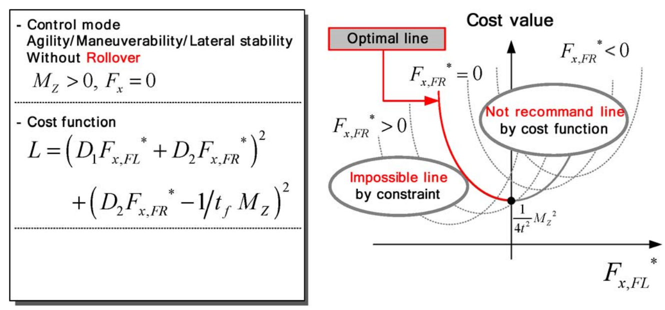


Fig. 12. Cost value in the yaw moment control without deceleration control: $Mz > 0$, and $Fx = 0$.

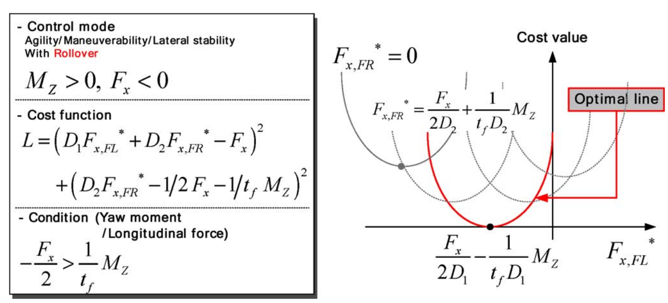


Fig. 13. Cost value in the yaw moment control with deceleration control: $Mz > 0$, $Fx < 0$, and $-1/2Fx > 1/2tf$ Mz.

desired yaw moment, the ESC system supplements the desired yaw moment.

If both the desired yaw moment for the lateral dynamics and the longitudinal force for the deceleration are needed in the current driving situation ($M_z > 0, F_x < 0$), the coordinator determines the actuator inputs by the first term of the cost function to minimize error between the desired longitudinal deceleration and the actual longitudinal deceleration. In addition, by the second term of the cost function, the differential braking of the braking force for obtaining the desired longitudinal force (not an additional actuator such as AFS) is preferentially used for the desired yaw moment and longitudinal force. In this case, only the ESC system is used to satisfy the desired yaw moment and longitudinal force. Fig. 13, which shows the cost value of the coordination, verifies the aforementioned contents.

However, if the desired yaw moment cannot be guaranteed only by differential braking for the longitudinal force, an insufficient desired yaw moment is generated by the AFS. Furthermore, if the desired yaw moment cannot be ensured by differential braking for the desired longitudinal force and the AFS, additional differential braking is used for the generation of the desired yaw moment. In this case, both the AFS and ESC systems are used to satisfy the desired yaw moment and longitudinal force. In addition, because additional braking for satisfying the desired yaw moment is used, longitudinal control for following the desired velocity cannot be ensured. Fig. 14 describes the aforementioned contents.

Based on (31) and (32), the Hamiltonian is defined as follows:

$$
\begin{aligned}
H =& \left(D_1 F_{x,FL}^* + D_2 F_{x,FR}^* - F_x\right)^2 \\
&+ \left(D_2 F_{x,FR}^* - \frac{F_x}{2} - \frac{1}{t_f} M_z\right)^2
\end{aligned}
$$

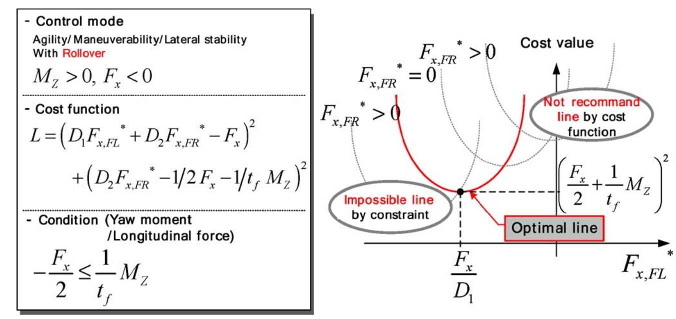


Fig. 14. Cost value in yaw moment control with deceleration control: $Mz > 0$, $Fx < 0$, and $-1/2Fx \leq 1/2tf$ Mz.

$$
\begin{aligned}
&+ \lambda_1 \left(-\frac{t_f}{2} D_1 F_{x,FL}^* + \frac{t_f}{2} D_2 F_{x,FR}^* + l_f E_1 F_{y,FL}^* - M_z\right) \\
&+ \rho_1 \left(F_{x,FL}^{*2} + \left(F_{y,FL} + F_{y,FL}^*\right)^2 - \mu^2 F_{z,FL}^2 + c_1^2\right) \\
&+ \rho_2 \left(F_{x,FR}^* + c_2^2\right)
\end{aligned} \tag{33}
$$

where $\lambda$ is the Lagrange multiplier, $c_1$ and $c_2$ are the slack variables, and $\rho_1$ and $\rho_2$ are semipositive values. The first-order necessary conditions about the Hamiltonian are determined using the KKT condition theory as

$$
\begin{aligned}
\frac{\partial H}{\partial F_{x,FL}^*} =& 2D_1 \left(D_1 F_{x,FL}^* + D_2 F_{x,FR}^* - F_x\right) - \frac{t_f}{2} D_1 \lambda_1 \\
&+ 2\rho_1 F_{x,FL}^* = 0 \\
\frac{\partial H}{\partial F_{x,FR}^*} =& 2D_1 \left(D_1 F_{x,FL}^* + D_2 F_{x,FR}^* - F_{x,des}\right) \\
&+ 2D_2 \left(D_2 F_{x,FR}^* - \frac{F_x}{2} - \frac{1}{t_f} M_z\right) \\
&+ tD_2 \lambda_1 + \rho_2 = 0 \\
\frac{\partial H}{\partial F_{y,FL}^*} =& l_f E_1 \lambda_1 + 2\rho_1 \left(F_{y,FL}^* + F_{y,FL}\right) = 0 \\
\frac{\partial H}{\partial \lambda_1} =& -\frac{t_f}{2} D_1 F_{x,FL}^* + \frac{t_f}{2} D_2 F_{x,FR}^* \\
&+ l_f E_1 F_{y,FL}^* - M_z = 0 \\
\rho_1 g_1(x) =& \rho_1 \left(F_{x,FL}^{*2} + \left(F_{y,FL}^* + F_{y,FL}\right)^2 - \mu^2 F_{z,FL}^2\right) = 0 \\
\rho_2 g_2(x) =& \rho_2 F_{x,FR}^* = 0.
\end{aligned} \tag{34}
$$

Based on the last line in (34), four cases are derived as follows:

$$\text{Case 1}: \rho_1 = 0,\ \rho_2 = 0 \ or\ g_1(x) < 0,\ g_2(x) < 0. \tag{35a}$$

$$\text{Case 2}: \rho_1 = 0,\ \rho_2 > 0 \ or\ g_1(x) < 0,\ g_2(x) = 0. \tag{35b}$$

$$\text{Case 3}: \rho_1 > 0,\ \rho_2 = 0 \ or\ g_1(x) = 0,\ g_2(x) < 0. \tag{35c}$$

$$\text{Case 4}: \rho_1 > 0,\ \rho_2 > 0 \ or\ g_1(x) = 0,\ g_2(x) = 0. \tag{35d}$$

Case 1 means that the sum of the longitudinal and lateral tire forces is smaller than the friction of the tire and it is possible to release the braking pressure. Case 2 means that the sum of the longitudinal and lateral tire forces is smaller than the friction

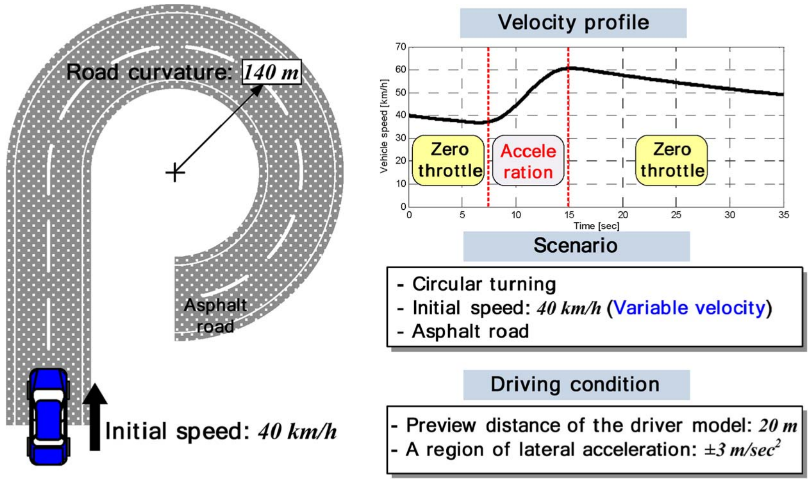


Fig. 15. Simulation scenario for evaluating agility performance.

of the tire and it is impossible to release the braking pressure. Case 3 means that the sum of the longitudinal and lateral tire forces is equal to the friction of the tire and it is possible to release the braking pressure. Case 4 means that the sum of the longitudinal and lateral tire forces is equal to the friction of the tire and it is impossible to release the brake pressure. The solutions of (34), i.e., $F^*_{x,FL}$, $F^*_{x,FR}$, and $F^*_{y,FL}$, are determined as follows:

Case 1

$$F^*_{x,FR} = \frac{1}{2D_2}\left(F_x + \frac{2M_z}{t_f}\right)$$
$$F^*_{x,FL} = \frac{1}{2D_1}\left(F_x - \frac{2M_z}{t_f}\right), \qquad F^*_{y,FL} = 0.$$

Case 2

$$F^*_{x,FL} = \frac{1}{D_1}F_x, F^*_{x,FR} = 0, F^*_{y,FL} = \frac{1}{l_f E_1}\left(M_z + \frac{t_f}{2}F_x\right).$$

Case 3

$$F^*_{x,FL} = \frac{-QP + \sqrt{\mu^2(1+Q^2)F^2_{z,FL} - P^2}}{(1+Q^2)}$$
$$F^*_{x,FR} = \frac{F_x - D_1 F^*_{x,FL}}{D_2}$$
$$F^*_{y,FL} = \frac{M_z - t_f/2F_x + t_f D_1 F^*_{x,FL}}{l_f E_1}$$
$$\text{where } P = \frac{M_z - \frac{t_f}{2}F_x + l_f E_1 F^*_{y,FL}}{l_f E_1}, \quad Q = \frac{t_f D_1}{l_f E_1}.$$

Case 4

$$F^*_{x,FL} = \frac{-\kappa\zeta + \sqrt{\mu^2(1+\kappa^2)F^2_{z,FL} - \zeta^2}}{1+\kappa^2} \qquad F^*_{x,FR} = 0$$
$$F^*_{y,FL} = \frac{t_f D_1}{2l_f E_1}F^*_{x,FL} + \frac{1}{l_f E_1}M_z$$
$$\text{where} \quad \kappa = \frac{t_f D_1}{2l_f E_1}, \zeta = \frac{1}{l_f E_1}M_z + F_{y,FL}. \tag{36}$$

The brake pressure of each wheel and the active steering angle are obtained using (36).

## VI. Evaluation

The proposed UCC system was evaluated through computer simulations using the vehicle simulation software CarSim and MATLAB/Simulink. Simulations for a closed-loop driver–vehicle–controller system subject to circular turning and single lane change were conducted to validate the improved performance of the proposed UCC system over the no-control system and the conventional UCC. The conventional UCC system is the integration system of the AFS and ESC as the proposed UCC system [19]. However, unlike the proposed UCC system, the conventional UCC system considered only the vehicle stability without agility and the sideslip angle. To classify the proposed and the conventional UCC systems, the conventional and the proposed UCC systems were called the UCC system and the advanced unified chassis control (AUCC) system, respectively.

The following two simulations were conducted to test the effectiveness of the proposed control system: 1) a circular turning simulation to evaluate the agility performance and 2) a single lane-change maneuver to evaluate the performance with respect to the sideslip angle. In these simulations, the steering wheel angle was determined by a driver steering model to describe the human driver's steering behavior in lane-following situations [20]. The steering wheel angle of the driver model can be determined using the vehicle velocity and the distance and heading angle errors between the reference path and the actual path of the vehicle.

### A. Cornering Simulation for Agility Control

A circular turning maneuver was simulated on an asphalt road. The initial vehicle speed was set to 40 km/h, and various throttle inputs were applied during the simulation. Fig. 15 shows a simulation scenario that consists of the reference trajectory, velocity profile, scenario, and driving condition. Because a simulation for the normal driving situation should

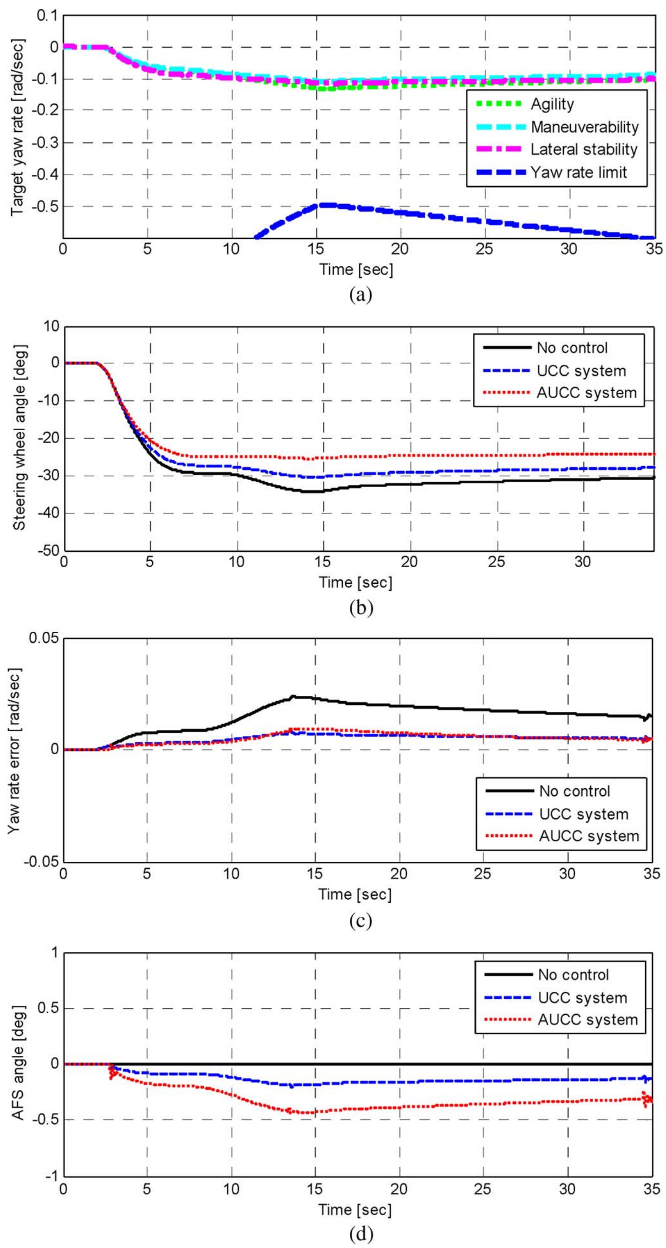


Fig. 16. Simulation results of a circular turning test. (a) Target yaw rates for control modes and yaw rate limit. (b) Steering wheel angle. (c) Yaw rate error. (d) AFS control input.

be conducted to evaluate the agility performance, the maximum lateral acceleration was limited to 3 m/s$^2$. In this paper, neutral steer was used to improve agility. In neutral steer, if the steering angle is set to a constant value, the vehicle can circle a constant road curvature, regardless of velocity.

As shown in the reference trajectory and velocity profile in Fig. 15, during cornering, the vehicle is accelerated at $= 7 \sim 13$ s and decelerated due to rolling resistance at $= 13 \sim 34$ s. Fig. 16 shows the simulation results for a circular turning test. Based on Fig. 16(a), it is known that agility control is activated by the AUCC system. Fig. 16(b)–(d) shows the steering wheel angle, yaw rate error, and control input of the AFS module, respectively. Because of the normal driving situation, the differential braking was not operated. All systems (no control, the UCC, and the AUCC) showed similar performance for vehicle stability, as shown Fig. 16(c). However, considering the relationship between the steering wheel angle and the vehicle trajectory, the AUCC system can follow a constant road curvature with a minimum steering angle and rate, as shown in Fig. 16(b).

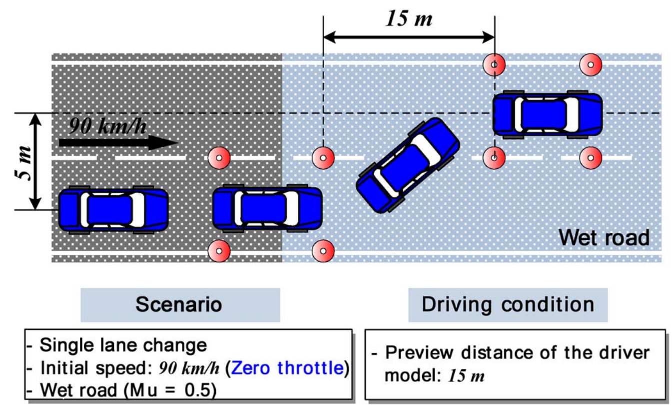


Fig. 17. Simulation scenario for evaluating the improvement in lateral stability.

### B. Lane-Change Simulation for Lateral Stability

To evaluate the lateral stability performance of the vehicle, a severe single lane-change maneuver was simulated on a wet road $(mu = 0.5)$. The initial vehicle speed was set to 90 km/h, and a zero throttle input was applied during the simulation. Fig. 17 shows a reference trajectory, the scenario, and the driving conditions.

Fig. 18 shows the single lane-change simulation results. If a control system is not applied, the yaw rate error and the sideslip angle of the vehicle diverge from the reference values, as shown in Fig. 18(c) and (d). If the UCC system is applied to the vehicle, the performance of vehicle dynamics for the yaw rate and the sideslip angle is better than the performance of the no-control system. However, as shown in the results for the sideslip angle, the sideslip angle for the UCC exceeded 0.1 rad/s at about 2 s. In the case of the UCC system, only the target yaw rate for maneuverability was used, as shown in Fig. 18(a). Because the AUCC system used the proposed target yaw rate, as shown in Fig. 18(b), the sideslip angle showed a good performance. Due to the small sideslip angle, the performance of the AUCC system was better than the UCC system, although small control inputs such as the AFS and the differential braking were used, as shown in Fig. 18(e) and (f).

## VII. Conclusion

A UCC strategy for improving agility, maneuverability, and lateral stability has been proposed to obtain the optimized coordination of individual ESC and AFS chassis control modules. The UCC system consists of the following three steps: 1) a supervisor for determining target vehicle motions such as yaw rate and velocity; 2) a control algorithm for determining the control inputs necessary to track the target vehicle motions; and 3) a coordinator for calculating actuator inputs such as the AFS angle and the braking pressure of each wheel. In the case of the

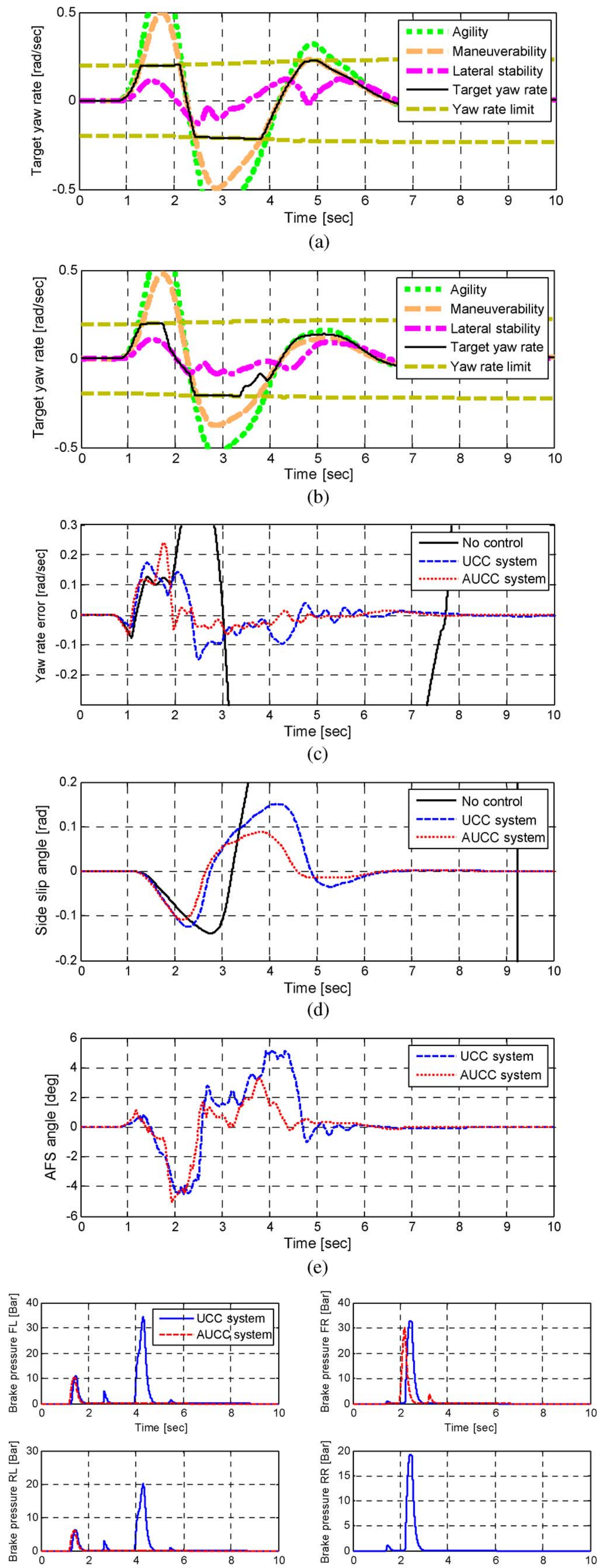


Fig. 18. Single lane-change simulation results. (a) Target yaw rate for the UCC system. (b) Target yaw rate for the AUCC system. (c) Yaw rate error. (d) Sideslip angle. (e) AFS control input. (f) Brake pressure.

coordinator, an optimization method using KKT conditions was applied to minimize a cost function. The optimization method used an objective function such as the deceleration minimization or actuation authority of the actuators while considering the specified performance limit for the actuator and tire.

The performance of the UCC system was investigated through closed-loop driver–vehicle–controller computer simulations. Based on the simulation results, it is confirmed that the proposed UCC system showed good performance for agility, maneuverability, and lateral stability compared with the UCC system studied in our previous research.

## REFERENCES


[1] B. A. Güvenç, T. Acarman, and L. Güvenç, "Coordination of steering and individual wheel braking actuated vehicle yaw stability control," in *Proc. IEEE Intell. Veh. Symp.*, 2003, pp. 288–293.

[2] W. J. Manning, M. Selby, D. A. Crolla, and M. D. Brown, "IVMC: Intelligent vehicle motion control," presented at the SAE World Congr. Exhib., Detroit, MI, 2002, Paper 2002-01-0821.

[3] M. Nagai, M. Shino, and F. Gao, "Study on integrated control of active front steering angle and direct yaw moment," *JSAE Rev.*, vol. 23, no. 3, pp. 309–315, Jul. 2002.

[4] Y. Kou, H. Peng, and D. Jung, "Development of an integrated chassis control system for worst case studies," in *Proc. AVEC*, 2006, pp. 47–52.

[5] A. Goodarzi and M. Alirezaie, "A new fuzzy-optimal integrated AFS/DYC control strategy," in *Proc. AVEC*, 2006, pp. 65–70.

[6] R. Kazemi, J. Ahmadi, A. Ghaffari, and M. Kabganian, "Vehicle yaw stability control through combined differential braking and active rear steering based on linguistic variables," in *Proc. AVEC*, 2006, pp. 661–666.

[7] X. Shen and F. Yu, "Investigation on integrated vehicle chassis control based on vertical and lateral tire behavior correlativity," *Veh. Syst. Dyn.*, vol. 44, pp. 506–519, 2006.

[8] J. Wang and R. G. Longoria, "Coordinated vehicle dynamics control with control distribution," in *Proc. Amer. Control Conf.*, 2006, pp. 5348–5353.

[9] D. Li, X. Shen, and F. Yu, "Integrated vehicle chassis control with a main/servo-loop structure," *Int. J. Autom. Technol.*, vol. 7, no. 7, pp. 803–812, Dec. 2006.

[10] O. Mokhiamar and M. Abe, "Simultaneous optimal distribution of lateral and longitudinal tire forces for the model following control," *Trans. ASME J. Dyn. Syst. Meas. Control*, vol. 126, no. 4, pp. 753–762, Dec. 2004.

[11] E. Ono, Y. Hattori, Y. Muragishi, and K. Koibuchi, "Vehicle dynamics integrated control for four-wheel-distributed steering and four-wheel-distributed traction/braking systems," *Veh. Syst. Dyn.*, vol. 44, no. 2, pp. 139–151, Feb. 2006.

[12] H. Smarkman, "Functional integration of active suspension with slip control for improved lateral vehicle dynamics," in *Proc. AVEC*, 2000, pp. 397–404.

[13] W. Cho, J. Yoon, S. Yim, B. Koo, and K. Yi, "Estimation of tire forces for application to vehicle stability control," *IEEE Trans. Veh. Technol.*, vol. 59, no. 2, pp. 638–649, Feb. 2010.

[14] E. Roghanian, M. B. Aryanezhad, and S. J. Sadjadi, "Integrating goal programming, Kuhn–Tucker conditions, and penalty function approaches to solve linear bilevel programming problems," *Appl. Math. Comput.195*, no. 2, pp. 585–590, 2008.

[15] J. Jo, S. You, J. Joeng, K. Lee, and K. Yi, "Vehicle stability control system for enhancing steerability, lateral stability, and roll stability," *Int. J. Autom. Technol.*, vol. 9, no. 5, pp. 571–576, Oct. 2008.

[16] J. Lee and K. Yi, "Coordinated control of steering torque and differential braking for vehicle lane departure avoidance," in *Proc. Korean Soc. Autom. Eng. Annu. Conf.*, 2010, pp. 1194–1201.

[17] S. You, J. Jo, S. Yoo, J. Hahn, and K. Lee, "Vehicle lateral stability management using gain-scheduled robust control," *J. Mech. Sci. Technol.*, vol. 20, no. 11, pp. 1898–1913, Nov. 2006.

[18] J. Yoon, W. Cho, B. Koo, and K. Yi, "Unified chassis control for rollover prevention and lateral stability," *IEEE Trans. Veh. Technol.*, vol. 58, no. 2, pp. 596–609, Feb. 2009.

[19] W. Cho, J. Yoon, J. Kim, J. Hur, and K. Yi, "An investigation into unified chassis control scheme for optimized vehicle stability and maneuverability," *Veh. Syst. Dyn.*, vol. 46, no. 1, pp. 87–105, 2008.

[20] J. Kang, K. Yi, S. Yi, and K. Noh, "Development of a finite optimal preview control-based human driver steering model," in *Proc. Korean Soc. Autom. Eng., Spring Conf.*, 2006, vol. 3, pp. 1632–1637.

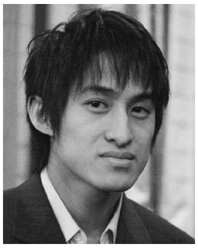

**Wanki Cho** received the B.S. degree in mechanical engineering in 2004 from Hanyang University, Seoul, Korea, and the M.S. degree in mechanical and aerospace engineering in 2006 from Seoul National University, where he is currently working toward the Ph.D. degree in mechanical and aerospace engineering with the School of Mechanical and Aerospace Engineering.

His research interests include the unified chassis control of a vehicle.

**Jaewoong Choi** received the B.S. degree in mechanical and aerospace engineering in 2007 from Seoul National University, Seoul, Korea, where he is currently working toward the Ph.D. degree in mechanical and aerospace engineering in the School of Mechanical and Aerospace Engineering.

His research interests include hybrid electric vehicle control, autonomous vehicle control, and intelligent vehicle safety systems.

**Chongkap Kim** received the B.S. degree in mechanical engineering from Hongik University, Seoul, Korea, in 1986.

He is currently a Senior Research Engineer with the Intelligent Vehicle Safety System Development Team, Hyundai Motor Company, Seoul. His research interests include integrated control systems in chassis and advanced driver-assistance systems.

**Seibum Choi** received the B.S. degree in mechanical engineering from Seoul National University, Seoul, Korea, in 1985, the M.S. degree in mechanical engineering from the Korea Advanced Institute of Science and Technology, Daejeon, Korea, in 1987, and the Ph.D. degree in mechanical engineering from the University of California, Berkeley, in 1993.

He is currently an Associate Professor with the Department of Mechanical Engineering, Korea Advanced Institute of Science and Technology.

**Kyongsu Yi** received the B.S. and M.S. degrees in mechanical engineering from Seoul National University, Seoul, Korea, in 1985 and 1987, respectively, and the Ph.D. degree in mechanical engineering from the University of California, Berkeley, in 1992.

From 1993 to 2005, he was with the School of Mechanical Engineering, Hanyang University, Seoul. He is currently a Professor with the School of Mechanical and Aerospace Engineering, Seoul National University. He currently serves as a Member of the Editorial Boards of the *Korean Society of Mechanical Engineers (KSME) Journal*, the *International Journal of Automotive Technology*, and the *ICROS Journal*. He is currently the Director of the Vehicle Dynamics and Control Laboratory. His research interests include control systems, driver-assistance systems, and active safety systems of a ground vehicle.

Dr. Yi is a member of the American Society of Mechanical Engineers, KSME, the Society of Automotive Engineers, and the Korean Society of Automotive Engineers. He received the PAEKAM Best Paper Award from the KSME in 1997 and the Acadecim Award from the KSAE in 2004.